

Freeze-out volume in multifragmentation - dynamical simulations

M. Pârlog^{1,2a}, G. Tăbăcaru^{3,2b}, J.P. Wieleczko¹, J.D. Frankland¹, B. Borderie³, A. Chbihi¹, M. Colonna^{4,5}, and M.F. Rivet³

¹ GANIL, CEA et IN2P3-CNRS, B.P. 5027, F-14076 Caen cedex, France.

² National Institute for Physics and Nuclear Engineering, RO-76900 Bucharest-Măgurele, Romania.

³ Institut de Physique Nucléaire, IN2P3-CNRS, F-91406 Orsay cedex, France

⁴ Laboratori Nazionali del Sud, via S. Sofia 44, I-95123 Catania, Italy.

⁵ Physics-Astronomy Department, University of Catania, Italy.

3rd September 2018

Abstract Stochastic mean-field simulations for multifragmenting sources at the same excitation energy per nucleon have been performed. The freeze-out volume, a concept which needs to be precisely defined in this dynamical approach, was shown to increase as a function of three parameters: freeze-out instant, fragment multiplicity and system size.

PACS. 2.1.30.Fe;25.70.-z;25.70.Lm;25.70.Pq;24.60.Ky; NUCLEAR REACTIONS $^{119}\text{Sn}(^{129}\text{Xe}, X)$, $E = 32$ AMeV; $^{238}\text{U}(^{155}\text{Gd}, X)$, $E = 36$ AMeV; central collisions; multifragmenting sources; stochastic mean-field simulations; dynamical evolution of the freeze-out volume.

1 Introduction

Several hundreds of nucleons may be brought into interaction in central heavy ion collisions around the Fermi energy. Such reactions are good candidates to provoke a liquid-gas type phase transition - conceivable given the nature of the nuclear force - and to break the system into massive fragments [1,2]. The volume of such a source of ejectiles at the instant when all of them become free of the attractive force and feel only the Coulomb repulsion - *the freeze-out volume* - brings information on the coexistence of phases. It is a key quantity [3] to be connected to the physical observables, asymptotically measured. If in the statistical models [4,5,6,7] it is a basic *a priori* hypothesis, in the following dynamical treatment this volume is provided - at a given available energy - as a family of results illustrating the temporal and spatial evolution of the source in multifragmentation.

Nuclear multifragmentation may occur when the source has expanded through the spinodal region of negative compressibility [1] of the liquid-gas coexistence domain, a scenario valid for other many-body systems too [8,9]. Related Stochastic Mean Field (SMF) approaches [10,11,12] consider, under different approximations, the amplification of density fluctuations, due to N-body correlations, by the unstable mean field leading to spinodal decomposition. The Brownian One-Body (BOB) dynamics version, simulating the fluctuations by means of a brownian force in the

mean field [13,14,15], coupled to Boltzmann-Nordheim-Vlasov (BNV) one-body density calculations [14], was successfully confronted with multifragmentation data measured with the 4π multidetector INDRA [16]. Two systems at close available energy per nucleon ~ 7 MeV, were experimentally studied: 32 AMeV $^{129}\text{Xe} + ^{nat}\text{Sn}$ and 36 AMeV $^{155}\text{Gd} + ^{nat}\text{U}$ [29,17,18,19,20,21,22]. The comparison between simulated events for central collisions - filtered according to the experimental features of INDRA - and the experimental data was recently extended from fragment multiplicity M , charge Z , largest charge Z_{max} and bound charge $Z_{bound} = \Sigma Z$ distributions [18] to charge [19,21] and velocity correlation functions and energy spectra [22]. The theoretical approaches developed in relation with the advanced experimental methods of nuclear physics may be esteemed in the new and more general physics of the phase transition in finite systems [3,8,23].

As a reasonably successful dynamical description of the multifragmentation process at intermediate bombarding energies, the above mentioned three dimensional (3D) SMF simulations provide a well adapted framework to address the question of the freeze-out volume. We focus in the present paper on disentangling the time, fragment multiplicity and source size of the freeze-out volume dependence. A pragmatical definition of the freeze-out instant is proposed.

^a Correspondence to: parlog@ganil.fr

^b Present address: Cyclotron Institute, Texas A&M University, College station, Texas 77845, USA

2 Expanding sources provided by BOB simulations

SMF simulations of nucleus-nucleus collisions based on the Boltzmann-Langevin equation were proposed to treat unstable systems [11,12,24] but their application to 3D nuclear collisions is prohibited by computational limitations. Instead, the spinodal decomposition of two diluted nuclear sources, mentioned above, at the same temperature (≈ 4 MeV), was mimicked through the BOB dynamics [13,15,18], applicable to locally equilibrated systems. The brownian force employed in the kinetic equations is grafted on to the one-body density evolution, calculated in a BNV approach [14], at the moment of maximum compression $t_0 \approx 40$ fm/c after the beginning of the collision, before the entrance of the system into the spinodal region. Its strength can be tuned to describe the growth of the most important unstable modes, ascribed to the density fluctuations, which need a short, but finite time to develop. The dispersion relation [25] puts them in evidence. It includes quantal effects and connects the characteristic time to its associated multipolarity. In turn, the multipolarity of the unstable collective modes, increasing with the size of the source, may be related to the fragment multiplicity [25,26]. The delimitation between fragments - the "liquid drops" - and light clusters - "the gas" - in which they are embedded is given by a cut-off value $\rho_{min} \geq 0.01 fm^{-3}$ of the nuclear density ρ [18].

The ingredients of the simulations, corresponding to zero impact parameter, as well as the selection criteria for the complete events from experimental central collisions, can be found in [18,27]. The fragments are defined as having the atomic number $Z \geq 5$. In the reported calculation, as in the experimental selection, only events having the final fragment multiplicity $M \geq 3$ were considered [18]. The calculated total charge of the multifragmenting sources in the spinodal zone, $Z_{tot} = 100$ for $^{129}\text{Xe} + ^{119}\text{Sn}$ and $Z_{tot} = 142$ for $^{155}\text{Gd} + ^{238}\text{U}$ are close to the experimentally reconstructed ones [18]; INDRA identifies the mass of the light charged products ($Z < 5$) but not that of the fragments. The Skyrme force used in our simulations is not isospin dependent. Consequently, the mass numbers of the sources: $A_{tot} = 238$ (for the light one) and $A_{tot} = 360$ (for the heavy one) correspond to the conservation of the entrance channel N/Z ratio. The charge distributions (normalized to the fragment multiplicity of the event) measured [28] or simulated in BOB calculations [18], are identical in the two cases - consistent with a bulk effect in the involved multifragmentation process.

Starting from the two initial partners of the reaction, the BNV calculation leads to a spherical distribution of matter. It undergoes a self-similar expansion, which is not dramatically altered by the BOB simulations - Fig. 1. The simulated sources continue their rather isotropical 3D expansion in time, no particularly elongated or flat shapes being produced. The concept of a radially symmetric freeze-out volume keeps its full sense, provided that the related instant may be singularized.

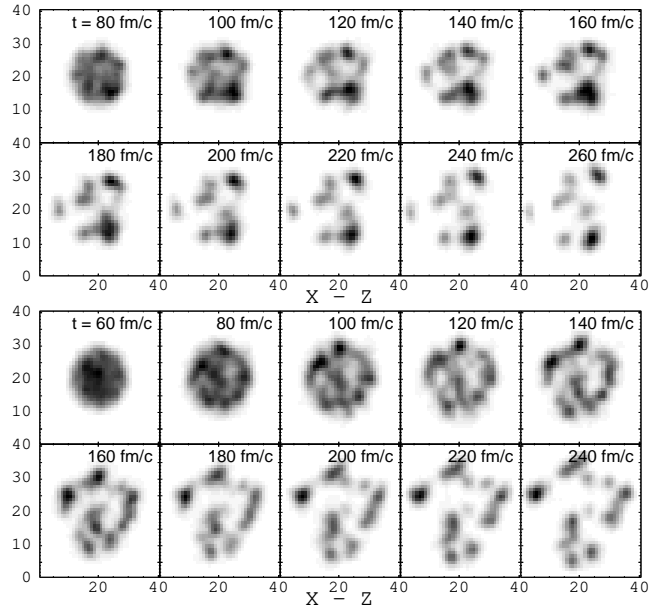


Figure 1. One event density evolution for each of the two multifragmenting sources: $A_{tot} = 238$ - upper panel - and $A_{tot} = 360$ - lower panel. The collision direction in the entrance channel is along Z axis and the unit is fm on both axes of these $X - Z$ views. The centre of mass coordinates are $X = Z = 20$ fm.

2.1 The freeze-out instant definition

The fragments are not all formed at the same moment, their mean multiplicity increasing in time, up to ~ 250 fm/c [18] when it saturates at a value of about 5 for the lighter source ($Z_{tot} = 100$, $A_{tot} = 238$) associated to the $\text{Xe} + \text{Sn}$ reaction, and of about 8 for the heavier one ($Z_{tot} = 142$, $A_{tot} = 360$) associated to the $\text{Gd} + \text{U}$ reaction. Indeed, even for the same final multiplicity of a source, there are events where the density fluctuations grow up faster and others where the process is slower. A question of definition appears related to the freeze-out instant. Our BOB calculations are recorded in steps of time $\Delta t = 20$ fm/c starting from t_0 . Each event is traced back in steps of 20 fm/c from its asymptotical configuration ($t \approx 250$ fm/c) of final multiplicity M to the moment when the fragment multiplicity decreases one unit. We define the freeze-out instant of an event as the moment when its *final* fragment multiplicity M was established. It means that if at $t_{i-1} = t_0 + (i-1)\Delta t$ the event has the multiplicity $M-1$ and at $t_i = t_0 + i\Delta t$ it reaches the final multiplicity M , t_i will be considered as freeze-out instant. All events which got their final multiplicity M at the moment t_i are treated together. Fig. 2 shows, as an example, the distribution of the moments $t = t_i$ at which the final multiplicity $M = 5$ was reached for the lighter source $A_{tot} = 238$: $t \in [120, 260]$ fm/c.

2.2 Freeze-out configurations

For the sake of simplicity, the fragments are considered as spheres of normal density, but the results are quite

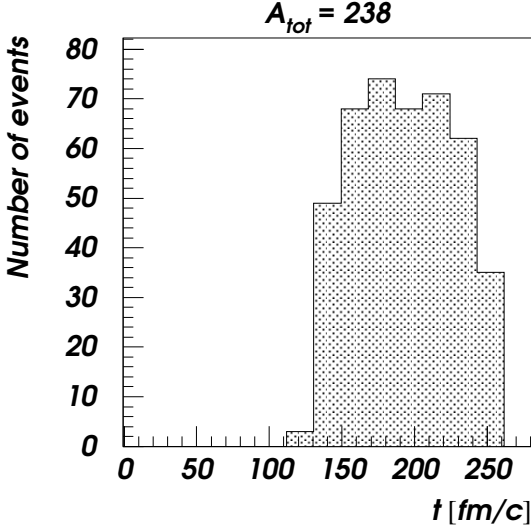


Figure 2. The distribution of the moments at which the final multiplicity $M = 5$ was reached for the source having $A_{tot} = 238$.

independent of this particular hypothesis. The relative distance d_{jk} between the surfaces of two fragments j, k ($j, k = 1 \div M$ and $j \neq k$) in one event, that will be called the intra-fragment distance in the following, is much varying for a given final multiplicity M : from a minimum of the order of 1 fm between the two most recently splitted fragments to a maximum value which increases with t . This behaviour is shown - for the source (100,238) and the multiplicity $M = 5$ - in the left-upper and left-middle panels of Fig. 3, at two different freeze-out instants: 180 and 240 fm/c. The distribution evolves towards larger distance values in time, from an asymmetric to a more symmetric shape. For the same two instants, the right-upper and right-middle panels of Fig. 3 present the distributions concerning the source (142,360) and $M = 8$. The evolution is similar to the lighter source case. Together with the lower panels, related to the freeze-out instant $t = 180$ fm/c and the multiplicity $M = 7$ for both sources, the upper graphs let also one see that, at the same moment ($t = 180$ fm/c), the mean value of the relative distance depends on M for a given source, while for different sources and the same multiplicity, e.g. $M = 7$, on the size of the source.

The distribution of the intra-fragment distances at a certain moment is quite illustrative for the momentary spatial configuration of the source: the shortest distances concern the first order neighbours, the longest ones the largest size of the sources and, above all, the intermediate values are qualitatively informing about the dilution of the source. The first and second order moments of the distribution and their dynamical evolution are appropriate to synthesize this last aspect. As expected, these quantities, analysed multiplicity by multiplicity, are increasing with

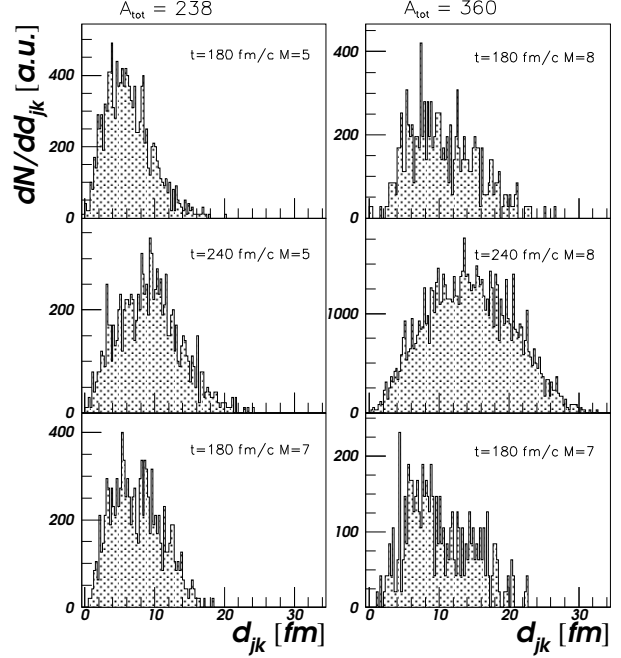


Figure 3. The distributions of relative distance d_{jk} between the surfaces of two fragments j, k , simulated event by event and related to two sources: $A_{tot} = 238$ - left column - and $A_{tot} = 360$ - right column, for various freeze-out instants and multiplicities.

increasing $t = t_i$, testifying on the enlargement of the matter distribution in the nuclear source in time. These values are higher for the heavier source than for the lighter one, and their increase in time seems to be slightly more pronounced. The fact has to be put in connection with the total Coulomb repulsion and the radial flow, higher for the heavier system than for the lighter one [18,22]. An interesting result is that, at constant values of $t = t_i$, the mean and the variance of intra-fragment distance distributions increase with the multiplicity - a little bit more accentuated for the lighter system. The slope of this dependence is higher at later moments t .

For each group of events reaching a final multiplicity M at a certain moment $t = t_i$, one may look for the corresponding local fragment concentration: dN/dV as a function of the vector radius absolute value r of the fragment position in the source reference framework. Examples of such distributions (at $t = 180$ and 240 fm/c) are given in the left-upper and left-middle panels of Fig. 4 for the lighter source and $M = 5$. When the same source and final multiplicity are involved, the mean radius \bar{r} and full width at half maximum ($FWHM$) increase with the time $t = t_i$ when the last two fragments are separated. In the right-upper and right-middle panels of Fig. 4 are represented - for the heavier source - the local fragment concentration distributions at these two moments and the final multiplicity $M = 8$. As previously, the distribution evolves in time towards larger radii; these radii are longer than in case of the lighter source. For the same final multiplicity: $M = 7$ and the same moment: $t = 180$ fm/c - the distri-

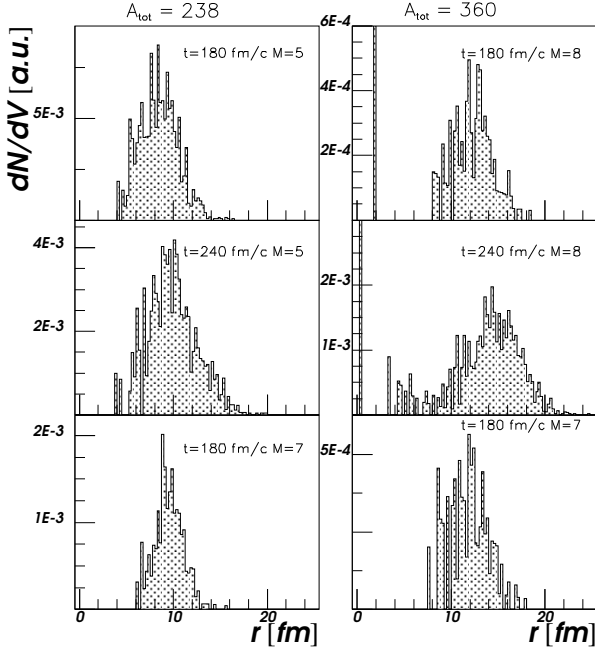


Figure 4. Radial distributions of the fragment concentration, simulated event by event and related to two sources: $A_{tot} = 238$ - left column - and $A_{tot} = 360$ - right column, for various freeze-out instants and multiplicities.

butions represented in the lower panels for both systems - the mean radius \bar{r} and $FWHM$ are longer in case of the heavier source. The upper and the lower panels together show that, for a given source at the same freeze-out instant, \bar{r} varies in the same sense as M .

Except the lowest multiplicity case for the lighter source, the radial distributions of the fragment concentration at the freeze-out instant are practically empty towards short radii, as shown in Fig. 4. They may be interpreted hence as reminiscences of bubble-like configurations.

3 The freeze-out volume

Once the freeze-out instant defined and the configurations when the latest formed fragments get free of nuclear interaction found, one may look for the corresponding volume. A sphere of radius $\bar{r} + FWHM/2$ englobes most of the fragment centres. Its volume - a good estimate of the quantity of interest - normalized at the volume $V_0 = (1.2)^3 A_{tot} \text{ fm}^3$ of the source at normal density ρ_0 , is considered as a function of the freeze-out instant $t = t_i$ at constant final multiplicity M of fragments. It is represented with full curves in the left column panels of Fig. 5 for the source $A_{tot} = 238$. The expansion of the source in time is evidenced: the dynamic process delivering the same final number M of fragments implies higher volumes if it takes place at later instants. These volumes increase from top to bottom with M , as well as the slopes of their variation. By adding to the above spheres the complements of fragment volumes which are exceeding them, one gains roughly 10%

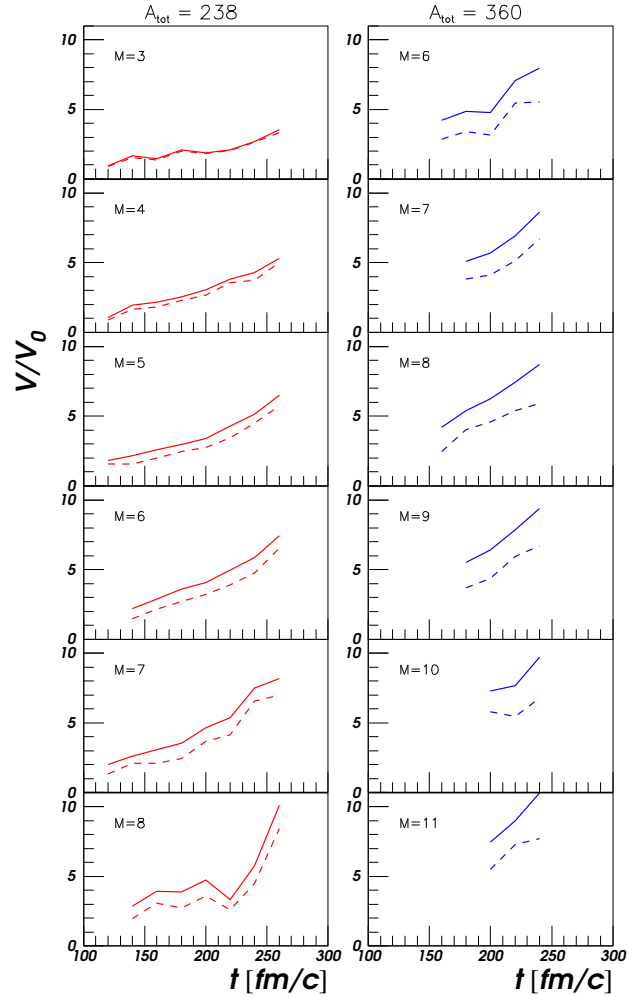


Figure 5. Freeze-out volumes as a function of the freeze-out instant, for two sources: $A_{tot} = 238$ - left column - and $A_{tot} = 360$ - right column. The full curves correspond to full spheres, while the dashed ones correspond to hollow spherical envelopes (see the text for explanations).

on the freeze-out values, but the general behaviour is not changed.

In fact, as shown in Fig. 4, the shapes of the fragment concentration distributions at freeze-out are generally gaussian like. About 75% of their integral is hence comprised between $\bar{r} - FWHM/2$ and $\bar{r} + FWHM/2$. The hollow envelopes delimited by the spheres with these radii are a kind of lower limits of the corresponding freeze-out volumes; always normalized at V_0 , they are drawn as dashed curves. The right column panels of Fig. 5 show similar results for the source $A_{tot} = 360$. The curves seem to rise slightly more rapidly than in the left column, in relation with the Coulomb effect and the radial flow.

The evolution with the multiplicity of the freeze-out volume defined above, calculated for full or hollow spheres and normalized at the volume of the corresponding source at normal density, is shown in Fig. 6 at given freeze-out moments. The dilution of the source increases with the fragment multiplicity - slightly faster for the lighter sys-

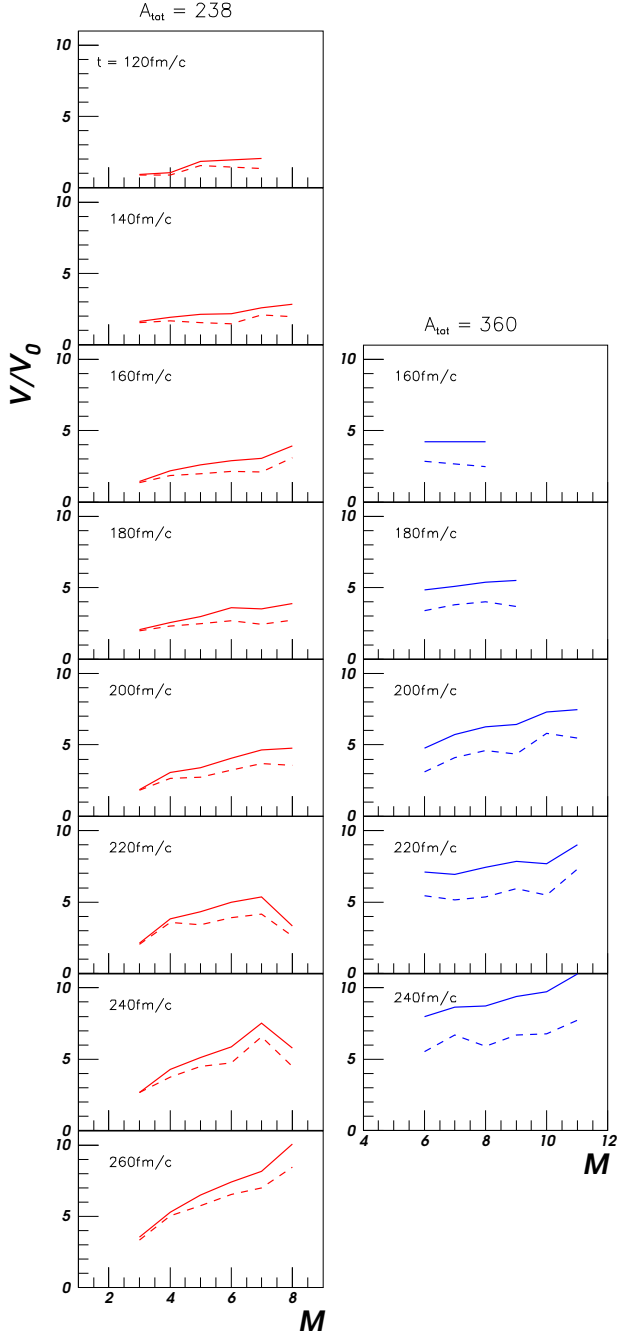


Figure 6. Freeze-out volumes as a function of multiplicity, at different freeze-out instants, for two sources $A_{tot} = 238$ - left column - and $A_{tot} = 360$ - right column. The full curves concern full spheres, while the dashed ones correspond to hollow spherical envelopes (see the text for explanations).

tem, presenting a higher relative variation of M (left column panels) than for the heavier one (right column panels); the variation is more pronounced at larger times. It reflects the mechanism considered here for the multifragmentation: the density fluctuations. The separation of the fragments in such an expanding source is reached on behalf of the lower density domains: the larger the number of

fragments, the larger the number of zones between them. Consequently, at the same freeze-out instant, the higher the multiplicity, the bigger the source volume. From the energetic point of view, a higher final fragment multiplicity M implies a higher fraction of the excitation energy consumed as binding (mainly surface) energy.

The freeze-out volumes provided by the present BOB calculation, averaged over time and multiplicity, are, of course, well fitting with those extracted, in the same framework, by using the mean multiplicity information. The corresponding densities ρ are compatible with the general prediction $\rho_0/10 < \rho < \rho_0/2$ of the Statistical Model for Multifragmentation (SMM) [5], in particular with the value $\rho_0/3$ used to study - in a nonsphericity hypothesis in this latter model - the fragment velocity correlations in the 32 A MeV $^{129}\text{Xe} + \text{nat}\text{Sn}$ system [29]. The present density values are lower than the average densities corresponding to the same domain of excitation energy, extracted from nuclear caloric curves [30,31]. The microcanonical model, analysing - all multiplicities together - the same multifragmenting systems [7], leads to volume values close to the present results but with a slightly lower dilution for the heavier system than for the lighter one.

The increase of the freeze-out volume with the basic experimental observable which is the fragment multiplicity in an event is more pronounced than that obtained when compacity criteria are used to fill the freeze-out domain in a static scenario. For the first time, reliable values as a function of time and final multiplicity are calculated. They give a dynamical image of the multifragmentation process at Fermi incident energies.

The final multiplicity of fragments is a measurable observable, while the time information is not directly accessible in the experiments. By weighting the freeze-out volume values got at different freeze-out instants with respect to the corresponding number of events, one may obtain a kind of average freeze-out volume at a given final multiplicity. This "time" averaged quantity, which loses

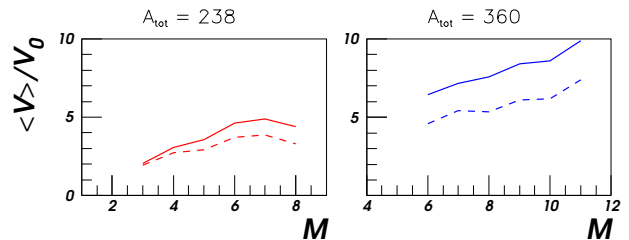


Figure 7. As in Fig. 6 but for "time" averaged freeze-out volumes; see the text for explanations.

much of its physical signification, indeed, is rapidly rising with M , as shown for the two sources in Fig. 7. The variety of fragment configurations, connected to the dynamical fluctuations of the system volume on the fragmentation path, has been recently related to monopole oscillations [9]. They may push the system towards a metastable configuration which eventually recontracts leading to low

fragment multiplicities, or develops into a hollow configuration which fragments at higher multiplicities.

4 Conclusions

Stochastic mean field simulations concerning the multifragmenting sources formed in 32 A MeV $^{129}\text{Xe} + ^{119}\text{Sn}$ and 36 A MeV $^{155}\text{Gd} + ^{238}\text{U}$ reactions have been performed. Their validity has already been checked [18, 19, 21, 22] by reproducing measurable physical observables determined for these reactions with the 4π multidetector INDRA. We found that the moment of separation of the latest two nascent fragments - the definition adopted for the freeze-out instant - is mainly distributed in the range $\sim (150 - 250)$ fm/c; multifragmentation is a dynamical process which is fast but needs a finite time. The topology of the associated freeze-out configurations are more complex but also more realistic as compared to the simplifying hypothesis in which the fragments, separated by a distance of the order of the nuclear interaction range, are forced to fill in a prescribed volume, as generally done in statistical codes.

The corresponding freeze-out volume could thus be disentangled in connection with the freeze-out instant, final fragment multiplicity and source size. For a given source and a given multiplicity, the evolution of this quantity illustrates the continuous expansion of the source in time. On the other hand, at the same freeze-out instant, the volume of one source increases with the fragment multiplicity, a basic measurable observable. As part of the energy associated to the internal degrees of freedom of the source is going along into fragment separation energy, its volume is dramatically increasing. And finally, for the same moment and the same multiplicity, the freeze-out volume is bigger for the heavier source, involving higher Coulomb repulsion and radial flow.

The dilution of a multifragmenting source, quantified as the ratio between its volume at freeze-out and its volume at normal density, is therefore increasing with time, fragment multiplicity and source size. Further SMF simulations, employing an isospin dependent nuclear force, would allow to study the isospin fractionation [32, 33], a phenomenon expected to be amplified at high source dilution. A comparative experimental investigation of isoscaling characteristics of these two systems prepared at the same available energy is desirable too.

References

1. G. F. Bertsch, P. J. Siemens, Phys. Lett. B **126**, 9 (1983).
2. L. G. Moretto and G. J. Wozniak, Phys. Rev. Ann. Rev of Nuclear and Particle science **43**, 379 (1993).
3. B. Borderie, J. Phys. G: Nucl. Phys. **28**, R217 (2002) and references therein.
4. D. H. Gross, Rep. Progr. Phys. **53**, 605 (1990); D. H. Gross, Phys. Rep. **279**, 119 (1997).
5. J. P. Bondorf, A. S. Botvina, A. S. Iljinov, I. N. Mishustin, K. Sneppen, Phys. Rep. **257**, 133 (1995).
6. J. A. Lopez, J. Randrup, Nucl. Phys. A **503**, 183 (1989); J. A. Lopez, J. Randrup, Nucl. Phys. A **512**, 345 (1990).
7. Al. H. Raduta, Ad. R. Raduta, Phys. Rev. C **65**, 054610 (2002).
8. P. Chomaz, M. Colonna and J. Randrup, "Nuclear spinodal fragmentation", Physics Reports 389, **5-6**, 263 (2004).
9. M. Colonna, G. Fabbri, M. Di Toro, F. Matera, H. H. Wolter, Nucl. Phys. A **742**, 337 (2004).
10. S. Ayik, C. Grégoire, Phys. Lett. B **212**, 269 (1988); S. Ayik, C. Grégoire, Nucl. Phys. A **513**, 187 (1990).
11. J. Randrup and B. Remaud, Nucl. Phys. A **514**, 339 (1990).
12. PH. Chomaz, G. F. Burgio and J. Randrup, Phys. Lett. B **254**, 340 (1991).
13. P. Chomaz, M. Colonna, A. Guarnera, J. Randrup, Phys. Rev. Lett. **73**, 3512 (1994).
14. A. Guarnera, M. Colonna, P. Chomaz, Phys. Lett. B **373**, 267 (1996).
15. A. Guarnera, P. Chomaz, M. Colonna, J. Randrup, Phys. Lett. B **403**, 191 (1997).
16. J. Pouthas, B. Borderie, R. Dayras, E. Plagnol, M.-F. Rivet, F. Saint-Laurent, J.-C. Steckmeyer, et al., Nucl. Instr. and Meth. in Phys. Res. A **357**, 418 (1995).
17. N. Marie, A. Chbihi, J. Natowitz, A. Le Fevre, S. Salou et al. (INDRA Collaboration), Phys. Rev. C **58**, 256 (1998).
18. J. D. Frankland et al. (INDRA Collaboration), Nucl. Phys. A **689**, 940 (2001).
19. B. Borderie et al. (INDRA Collaboration), Phys. Rev. Lett. **86**, 3252 (2001).
20. S. Hudan et al. (INDRA Collaboration), Phys. Rev. C **67**, 064613 (2003).
21. G. Tabacaru et al., Eur. Phys. J. A **18**, 103 (2003).
22. G. Tabacaru, Thèse de Doctorat Université Paris-XI Orsay (2000), IPNO T 00-13, <http://tel.ccsd.cnrs.fr/documents/archives0/00/00/79/12>.
23. F. Gulminelli, "Phase coexistence in nuclei", LPCC 03-06
24. G. F. Burgio, P. Chomaz and J. Randrup, Nucl. Phys. A **529**, 157 (1991).
25. S. Ayik, M. Colonna and P. Chomaz, Phys. Lett. B **353**, 417 (1995).
26. M. Colonna, P. Chomaz and S. Ayik, Phys. Rev. Lett. **88**, 122701 (2002).
27. J. D. Frankland et al. (INDRA Collaboration), Nucl. Phys. A **689**, 905 (2001).
28. M. F. Rivet et al. (INDRA Collaboration), Phys. Lett. B **430**, 217 (1998).
29. S. Salou, Thèse de Doctorat Université de Caen (1997), GANIL T 97 06, <http://tel.ccsd.cnrs.fr/documents/archives0/00/00/36/88>.
30. J. B. Natowitz et al., Phys. Rev. C **66**, 031601(R) (2002).
31. L. G. Sobotka et al., Phys. Rev. Lett. **93**, 132702 (2004).
32. V. Baran et al., Nucl. Phys. A **632**, 287 (1998).
33. Ph. Chomaz, F. Gulminelli, Phys. Lett. B **447**, 221 (1999).